

MOTION CHARACTERISTIC EVALUATION OF AN AMPHIBIOUS SPHERICAL ROBOT

Yanlin He,^{*,**} Shuxiang Guo,^{*,**} Liwei Shi,^{*,**} Huiming Xing,^{*,**} Zhan Chen,^{*,**} and Shuxiang Su^{*,**}

Abstract

This paper used three on-land locomotion gaits and underwater swim for an amphibious spherical robot, which is controlled using a closed-loop method. The aim of varying the on-land gaits and underwater swim was to improve the motion performance and stability of robot. To control the angle of joint, the displacement and depth of robot, a PID method was used to control the robot. Adams and MATLAB/SIMULINK were used to set the control parameters; simulation results are presented for the three on-land locomotion gaits and underwater swim, in terms of the motion performance, stability, and velocity of the robot. Finally, the effectiveness of the proposed methods was demonstrated by showing that the on-land and underwater horizontal motion was stable.

Key Words

Amphibious spherical robot, PID control, co-simulation, locomotion gaits, stability and autonomy

1. Introduction

Researchers around the world have been inspired by amphibians to develop amphibious robots. Wheeled robots perform well on even ground, whereas tracked and legged robots have good mobility on rough terrain. Compared with screw propellers, undulatory and oscillatory propulsion mechanisms disturb the environment only slightly and are highly efficient and manoeuvrable. Some robots utilize two sets of propulsion mechanisms for their terrestrial and aquatic motions, which makes them heavy. To simplify the structure, robots like Whegs and AQUA2 use a composite propulsion mechanism to move in amphibious environments [1], [2]. However, it is still difficult for these amphibious robots to move in complex terrains;

additionally, accurate control over the underwater position remains a challenge. To overcome the limitations of these amphibious robot, we developed a three-dimensional (3D) printing technology-based amphibious spherical robot with transformable composite propulsion mechanisms [3]–[6]. The robot is capable of moving from the water to the ground without manual intervention, and *vice versa* [4]–[9].

There is already extensive literature concerning on-land gaits of quadruped robots, including the crawling gait, trotting gait, *etc.*; these modes enable the robot to move efficiently and remain stable in different environments. The literature covers a range of issues such as modelling and adaptive gait transition, and a number of mechanisms to control these robots have been investigated, and many studies have been conducted on robot design, modelling, and control [10]. However, there are no accurately controllable robots capable of performing a range of land-based gaits and underwater movements with a water-jet propeller, with a composite mechanism designed to switch between the water-jet propeller and legs.

To have better adaptability and performance of amphibious motion in our robot, we used three locomotion gaits guided by a closed-loop controller to ensure that the motion remained stable. A PID closed-loop method is used to control the robot. We confirmed the correctness of the proposed method using Adams and MATLAB/SIMULINK, which we used to demonstrate the stability of amphibious movements. This enabled us to determine parameters for controlling the robot, as well as guided our selection of practical tests. We describe experiments in which we investigated three on-land gaits on a common mat floor. The choice of these experiments was guided by our simulation results. Underwater experiments were conducted to examine the performance of the robot as it moved horizontally.

The paper is organized as follows. Section 2 describes the design of robot. In Section 3, three on-land gaits are described, and the PID controllers were designed to facilitate co-simulation of on-land motion of robot. Section 4 is dedicated to the cooperative simulation of underwater motion. Some amphibious experimental is discussed in Section 5. Finally, Section 6 presents our conclusion.

* The Key Laboratory of Convergence Medical Engineering System and Healthcare Technology, the Ministry of Industry and Information Technology, School of Life Science, Beijing Institute of Technology, Beijing 100081, China; e-mail: {heyianlin, guoshuxiang, shimiwei, xinghuiming, chenzhan, sushuxiang}@bit.edu.cn

** Faculty of Engineering, Kagawa University, 2217-20 Hayashicho, Takamatsu, Kagawa 761-0396, Japan
Corresponding authors: Shuxiang Guo and Liwei Shi

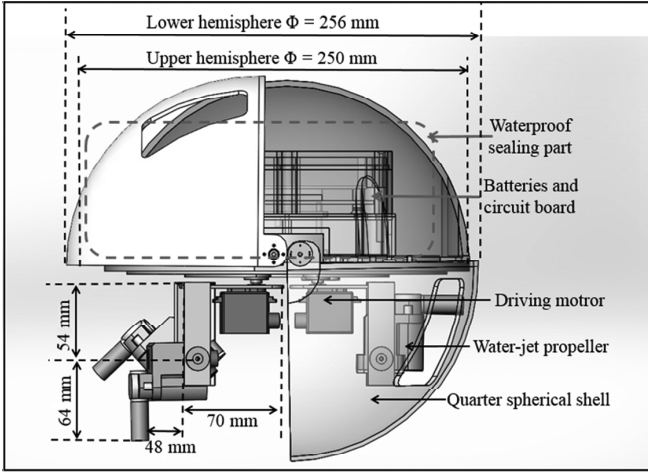


Figure 1. Structure of the amphibious spherical robot.

2. General Design of Amphibious Spherical Robot

In our previous research, we developed an amphibious spherical robot capable of motion on land and underwater. The design of the robot is shown in Fig. 1, which is able to move from underwater to the ground without manual intervention, and *vice versa*. The robot is composed of two sealed transparent upper hemispheroids, two openable transparent quarter spherical shells, and four actuating units, each of which consists of a water-jet propeller and two driving motors [3]–[13].

We used 3D printing technology, a minimal Xilinx Zynq-7000 SoC system, and an embedded computer equipped with an Intel Atom processor to fabricate the robot. We used an Avnet MicroZed core-board carrying a Xilinx all-programmable Zynq-7000 SoC, which is a hybrid processor combined with an advanced RISC machine processor and field-programmable gate array. The microcontroller provides eight pulse-width modulation (PWM) signals to control the servomotors; four PWM signals are used to actuate the water-jet propellers by regulating the signal duty ratio, and there are 12 general purpose input–output signals to control the optocoupler and relay [14].

3. On-Land Locomotion Gaits and Co-Simulation Analysis

3.1 On-Land Gait Characterization

We have implemented three on-land gaits for our robot [15]. Figure 2 shows the event sequences of a one-gait cycle

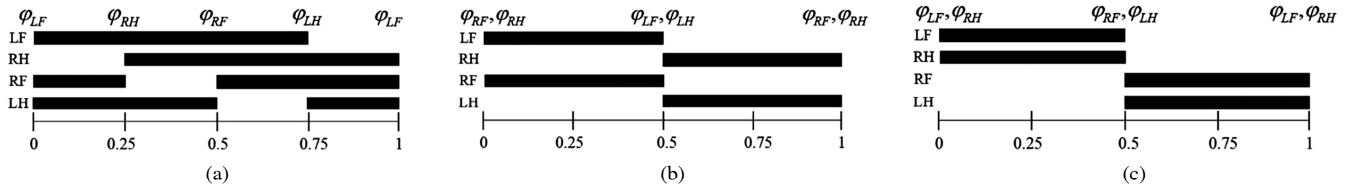


Figure 2. Event sequence of one gait cycle for each of the gaits: (a) crawling; (b) trotting; and (c) pacing.

for each of the three gaits. The shadow indicates that the legs are in contact with the ground. The legs are labelled as follows: left front (LF), right front (RF), left hind (LH), and right hind (RH). The duty factor of the crawling gait is $\beta = 0.75$; the duty factor of the trotting and pacing gaits is $\beta = 0.5$. There are times when the robot only has two legs in contact with the ground.

The velocity of the robot is related to the step size and cycle of the gait as follows [6]:

$$v = \frac{0.1483 * \theta}{T * \beta}, \quad (1)$$

where v is the velocity, T is the motion cycle, β is the duty factor, and θ is the rotation angle of hip joint.

3.2 On-Land Mathematical Modelling

As the movement mechanisms of four legs are essentially the same, we present the analysis of RF leg. As shown in Fig. 3, the inertial coordinate frame with respect to the ground was denoted XYZ , the body fixed coordinate system $\{X_b, Y_b, Z_b\}$ has its origin $\{O_b\}$ located in the geometric centre of robot. Assuming that the position vector of the rotational axes of the hip joint in the coordinate is $\{X_0, Y_0, Z_0\}$, the position vector of the rotational axes of the knee joint in the coordinate is $\{X_2, Y_2, Z_2\}$, and the relationship between rotational axes of the actuators with respect to body fixed coordinate can be obtained according to the homogeneous transformation matrix. Each leg is composed of a hip joint, a knee joint, and connecting

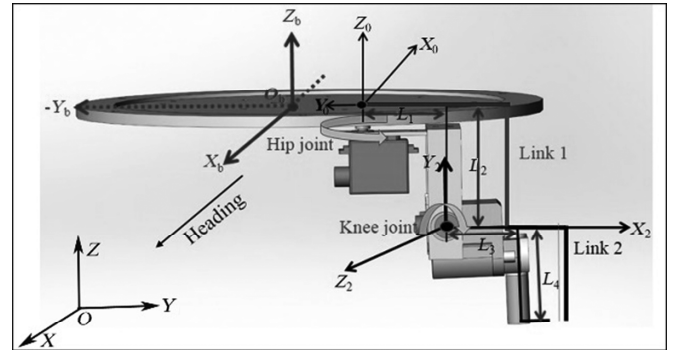


Figure 3. Force analysis and coordinate system of the amphibious spherical robot on land.

components. The dynamic Lagrange equation of robot is given below [16]:

$$L = E_k - E_p = \left[\frac{1}{2}(m_1 + m_2)v_1^2 + \frac{1}{2}(m_3 + m_4)v_2^2 \right] + (m_1 + m_2)gl_2 + (m_3 + m_4)g(l_2 + l_3 \cos \theta_2 + l_4 \sin \theta_2) \quad (2)$$

where E_k and E_p are the total kinetic and potential energies; m_1 and m_2 are the corresponding qualities of l_1 and l_2 ; m_3 and m_4 are the corresponding qualities of l_3 and l_4 ; and θ_1 and θ_2 are generalized coordinate variables.

The torque of the joint can be expressed as follows:

$$T_i = \frac{d}{dt} \frac{\partial L}{\partial \dot{\theta}_i} - \frac{dL}{d\theta_i} \quad (3)$$

The driving torques of the hip joint (T_1) and knee joint (T_2) are as follows:

$$D_{22} = \frac{1}{2} \left(\sum_{i=3}^4 m_i \right) (2l_3^2 s^2 \theta_2 + 2l_4^2 c^2 \theta_2 - 2l_3 l_4 s 2\theta_2) \quad (8)$$

$$D_{211} = -\frac{1}{2}(m_3 + m_4)(l_3^2 s 2\theta_2 - l_4^2 s 2\theta_2 + 2l_1 l_3 c \theta_2 - 2l_3 l_4 c 2\theta_2 + 2l_1 l_4 s \theta_2) \quad (9)$$

$$D_{211} = \frac{1}{2}(m_3 + m_4)(2l_3^2 s 2\theta_2 - 2l_4^2 s 2\theta_2 - 4l_3 l_4 c \theta_2 - l_3^2 s 2\theta_2 + l_4^2 s 2\theta_2 + 2l_3 l_4 s 2\theta_2) \quad (10)$$

$$D_{112} = D_{121} = \frac{1}{2}(m_3 + m_4)(l_3^2 s 2\theta_2 - l_4^2 s 2\theta_2 + 2l_1 l_3 c \theta_2 - 2l_3 l_4 c 2\theta_2 + 2l_1 l_4 s \theta_2) \quad (11)$$

$$D_2 = -2g(l_4 c \theta_2 - l_3 s \theta_2) \quad (12)$$

$$T_1 = \frac{d}{dt} \frac{\partial L}{\partial \dot{\theta}_1} - \frac{dL}{d\theta_1} = [(m_1 + m_2 + m_3 + m_4)l_1^2 + (m_3 + m_4)(l_3^2 \sin^2 \theta_2 + l_4^2 \cos^2 \theta_2 + 2l_1 l_3 \sin \theta_2 - l_3 l_4 \sin 2\theta_2 - 2l_1 l_2 \cos \theta_2)] \ddot{\theta} + [(m_3 + m_4)(l_3^2 \sin 2\theta_2 - l_4^2 \sin 2\theta_2 + 2l_1 l_3 \cos \theta_2 - 2l_3 l_4 \cos 2\theta_2 + 2l_1 l_4 \sin \theta_2 \dot{\theta}_1)] \quad (4)$$

$$T_2 = \frac{d}{dt} \frac{\partial L}{\partial \dot{\theta}_2} - \frac{dL}{d\theta_2} = \frac{1}{2}(m_3 + m_4)[(2l_3^2 \sin^2 \theta_2 + 2l_4^2 \cos^2 \theta_2 - 2l_3 l_4 \sin 2\theta_2) \ddot{\theta}_2 - (l_3^2 \sin 2\theta_2 - l_4^2 \sin 2\theta_2 + 2l_1 l_3 \cos \theta_2 - 2l_3 l_4 \cos 2\theta_2 + 2l_1 l_4 \cos 2\theta_2 + 2l_1 l_4 \sin \theta_2) \dot{\theta}_1^2 + (l_3^2 \sin 2\theta_2 - l_4^2 \sin 2\theta_2 - 2l_3 l_4 \cos 2\theta_2 + 2l_3 l_4 \cos 2\theta_2) \dot{\theta}_2^2 - 2g(l_4 \cos \theta_2 - l_3 \sin \theta_2)] \quad (5)$$

These general equations have been simplified and can be represented in simple matrix forms:

$$\begin{bmatrix} T_1 \\ T_2 \end{bmatrix} = \begin{bmatrix} D_{11}(\theta_2) & D_{12}(\theta_2) \\ D_{21}(\theta_2) & D_{22}(\theta_2) \end{bmatrix} \begin{bmatrix} \ddot{\theta}_1 \\ \ddot{\theta}_2 \end{bmatrix} + \begin{bmatrix} D_{111}(\theta_2) & D_{122}(\theta_2) \\ D_{211}(\theta_2) & D_{222}(\theta_2) \end{bmatrix} \begin{bmatrix} \dot{\theta}_1^2 \\ \dot{\theta}_2^2 \end{bmatrix} + \begin{bmatrix} D_{112}(\theta_2) & D_{122}(\theta_2) \\ D_{212}(\theta_2) & D_{221}(\theta_2) \end{bmatrix} \begin{bmatrix} \dot{\theta}_1 \dot{\theta}_2 \\ \dot{\theta}_1 \dot{\theta}_2 \end{bmatrix} + \begin{bmatrix} D_1 \\ D_2 \end{bmatrix} \quad (6)$$

where D_{11} and D_{22} are the effective inertia; D_{12} and D_{21} are the coupling inertia; D_{111} , D_{122} , D_{211} , and D_{222} are the coefficients of the centripetal acceleration; D_{112} , D_{121} , D_{212} , and D_{221} are the coefficients of the coriolis acceleration; and D_1 and D_2 are the gravity terms.

$$D_{11} = \left[\left(\sum_{i=1}^4 m_{i4} \right) l_1^2 + (m_3 + m_4)(l_3^2 s^2 \theta_2 + l_4^2 c^2 \theta_2 + 2l_1 l_3 s \theta_2 - l_3 l_4 s 2\theta_2 - 2l_1 l_2 c \theta_2) \right] \quad (7)$$

3.3 On-Land Control System Design and the Process of Co-Simulation

This section describes the modelling of robot in Adams. The 3D model of robot was simplified in SolidWorks and saved as (*.xt) format, and then the model was imported into Adams; some parameters were redefined and some constraints were applied. The initial state of robot was set as four-footed and assumed to be motioning on a ground; the contact force between the foot end and ground was set as friction force. Considering the experiments environment, the dynamic/static coefficient of friction force

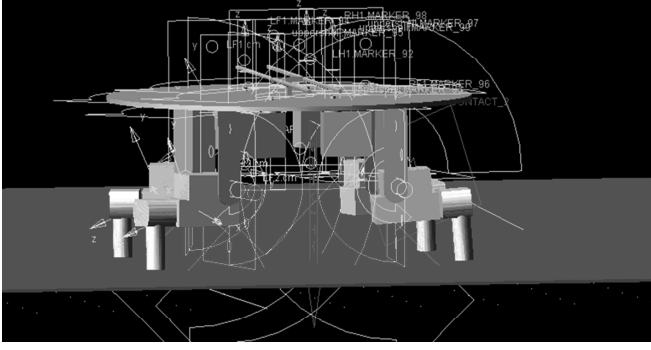


Figure 4. Virtual prototype of the robot developed using the Adams platform.

was set as 0.1/0.15, and the red portion in Fig. 4 represents the ground.

Eight driving torques were set as input variables in the co-simulation and can be expressed by the following equation:

$$T = [\text{Torque}_{\text{LF1}}, \text{Torque}_{\text{LF2}}, \text{Torque}_{\text{LH1}}, \text{Torque}_{\text{LH2}}, \text{Torque}_{\text{RF1}}, \text{Torque}_{\text{RF2}}, \text{Torque}_{\text{RH1}}, \text{Torque}_{\text{RH2}}] \quad (13)$$

where T_{LF1} , T_{LF2} , T_{LH1} , T_{LH2} , T_{RF1} , T_{RF2} , T_{RH1} , and T_{RH2} are the single-component torques of hip/knee joint of the

LF/RF/hind leg. The eight output swing angle variables of each joint can be expressed as follows:

$$A = [\text{Angle}_{\text{LF1}}, \text{Angle}_{\text{LF2}}, \text{Angle}_{\text{LH1}}, \text{Angle}_{\text{LH2}}, \text{Angle}_{\text{RF1}}, \text{Angle}_{\text{RF2}}, \text{Angle}_{\text{RH1}}, \text{Angle}_{\text{RH2}}] \quad (14)$$

where A_{LF1} , A_{LF2} , A_{LH1} , A_{LH2} , A_{RF1} , A_{RF2} , A_{RH1} , and A_{RH2} are defined as the swing angles of the hip/knee joint of the LF/RF/hind leg.

We used PID algorithm to control the velocity of joint, and its driving torque can be expressed as follows:

$$T = k_p e + k_d \dot{e} + k_i \int e dt \quad (15)$$

where T is the driving torque of joint; k_p , k_i , and k_d are the proportionality, differential, and differential coefficients; and e is the difference between the intended angle and actual angle.

There are eight input and eight output in the sub-system. The angle of joint is used as feedback and measured in Adams; through a mathematical operation, the displacement and velocity of joint can be determined, and a closed-loop control system was developed. Details of the control system are shown in Fig. 5 [17]–[22]; we can set different on-land locomotion gaits in MATLAB and measure their results.

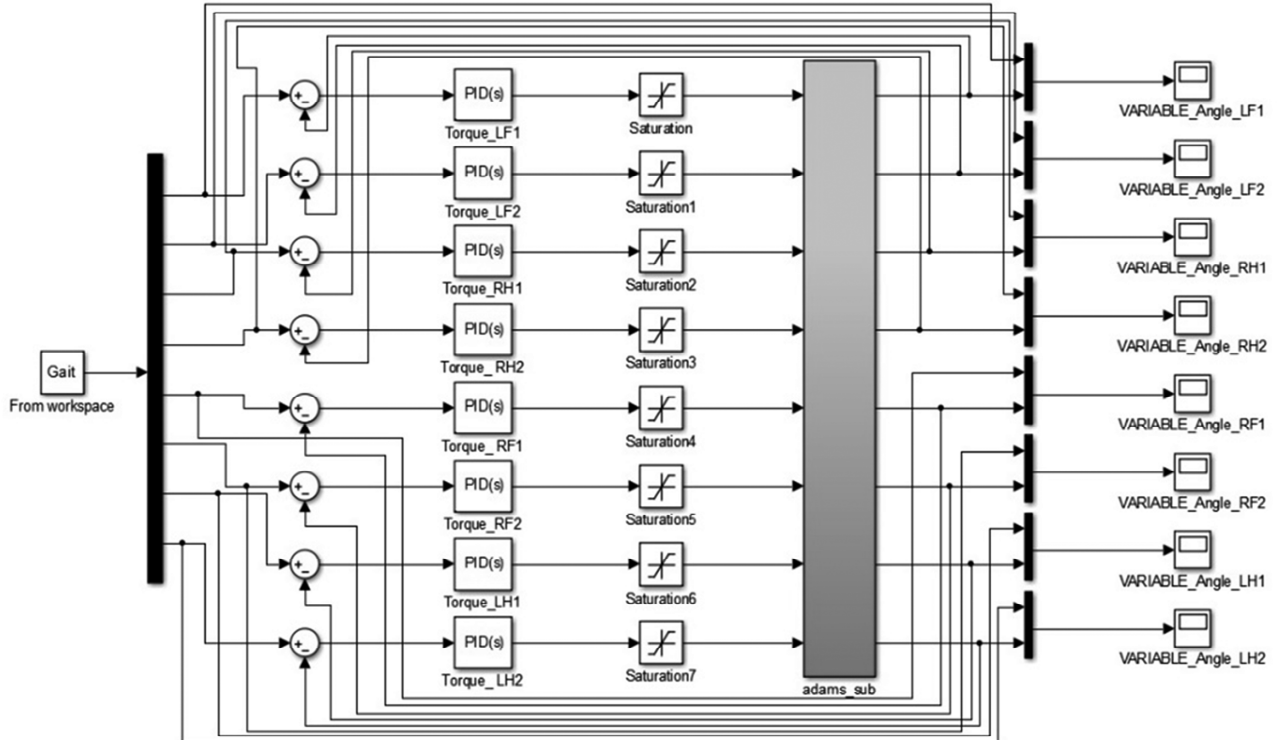


Figure 5. Structure of the co-simulation.

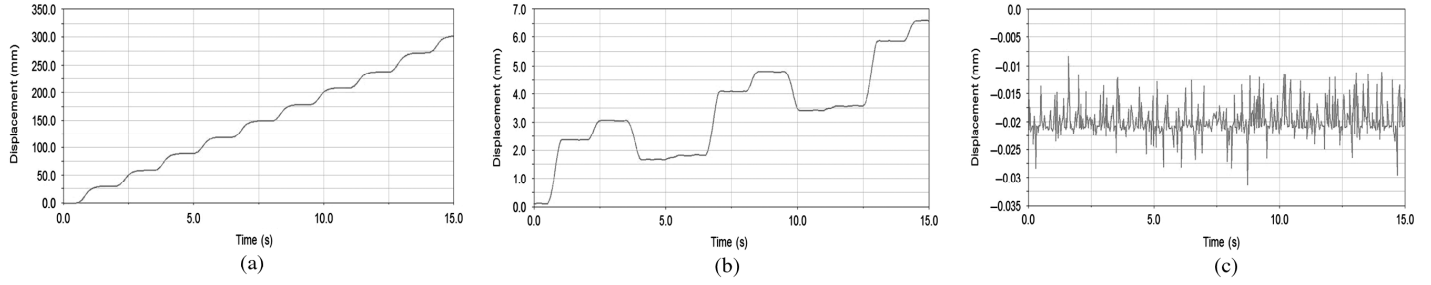


Figure 6. Displacement of the centroid of the robot as it moves with crawling gait: (a) X -axis direction; (b) Y -axis direction; and (c) Z -axis direction.

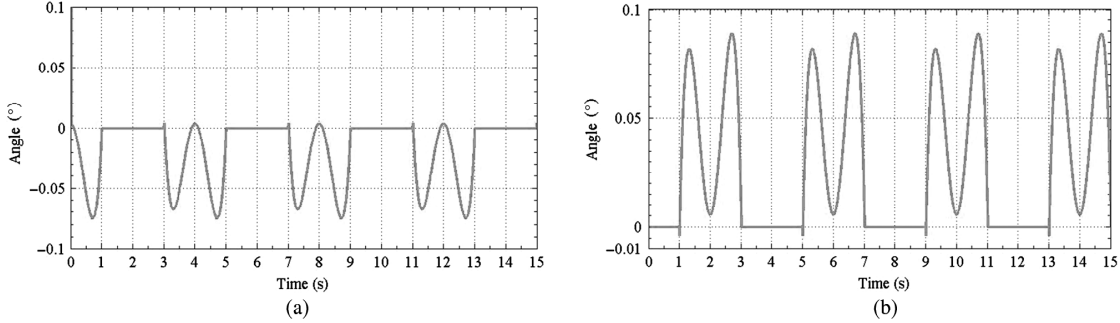


Figure 7. Tracking error of joint as the robot moves with crawling gait: (a) hip joint and (b) knee joint.

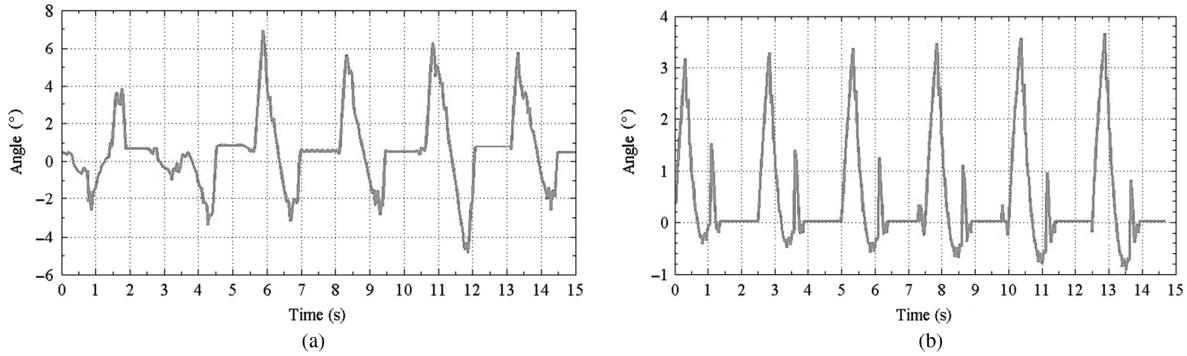


Figure 8. Tracking error of joint as the robot moves with trotting gait: (a) hip joint and (b) knee joint.

3.4 Co-Simulation Results and Analysis of Three On-Land Gaits

First, we studied the crawling gait and created a simulation of control system in MATLAB/SIMULINK, and then adjusted the control parameters of robot; the trajectory of the centroid of robot in three directions are presented in Fig. 6. In Fig. 6(a), we see that the change in X -direction is relatively stable, and the velocity of robot is around 20 mm/s. Figure 6(b) shows the deviation displacement in Y -direction; the maximum deviation of robot was approximately 6.2 mm, which is about 2.4% of the height of robot. Figure 6(c) shows the vibration in Z -direction; the maximum translocations is 0.028 mm, which is about 0.01% of the height of robot. Thus, the PID control is an effective method for controlling the crawling gait of robot.

The trajectory tracking error of hip and knee joints when guided by PID are shown in Fig. 7. In Fig. 7(a), except the maximum tracking error (0.08 mm) caused by the instantaneous driving force when the hip joint swings, the tracking error is small and tends to zero in other time periods. In Fig. 7(b), the tracking error of knee joint is closed to zero too. Consequently, the proposed control methods are able to track the intended trajectory of each joint when the robot moves with crawling gait.

From the trajectory results of the centroid of robot in the three directions with trotting gait, the velocity of robot is 43.3 mm/s; the maximum deviation is 9.8 mm. The maximum translocation is approximately 0.035 mm. The trajectory tracking errors of hip and knee joints are shown in Fig. 8; as we can see, with the exception of several individual large errors caused by the joints swing, the tracking error is minor.

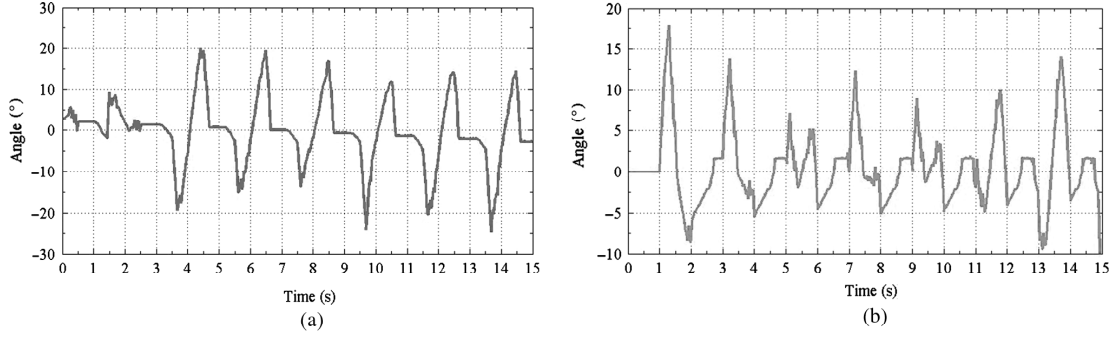


Figure 9. Tracking error of joint as the robot moves with pacing gait: (a) hip joint and (b) knee joint.

The results showed that the pacing velocity of robot was 50 mm/s, the maximum deviation of robot was approximately 88 mm, and the translocation remained at approximately 0.037 mm. The maximum errors in the hip and knee joints were approximately 20° and 18°, as shown in Fig. 9. Although the pacing gait were not stable as for the crawling and trotting gaits, the final trajectory was still essentially as desired.

4. Underwater Movement and Co-Simulation Analysis

When the robot in underwater environment, the four vectored propellers can change the directions and propulsive forces of its. We carried out force analysis on an actuator unit performing motions; and based on the leverage principle, we measured the thrust of a water-jet propeller for better control [3]–[6]. The results showed that the thrust increases as the input voltage increases, and at the maximum voltage of 16 V, the maximum thrust in two spray directions were 58.2 mN and 38.8 mN. At a voltage of 8 V, the maximum thrust in two spray directions were 13.4 mN and 6.4 mN [23].

4.1 Underwater Control System Design and the Process of Co-Simulation

When the robot moves in the horizontal direction, we mainly control its displacement and yaw angle [24]. As shown in Fig. 10, α_i and α_o are the input and output angles of robot, respectively. r_i and r_o are the displacement input and output of robot, respectively. The driving force and torque are given as follows:

$$M_{Ti} = k_{p1}(\alpha_i - \alpha_o) + k_{d1} \frac{d}{dt}(\alpha_i - \alpha_o) + k_{i1} \int (\alpha_i - \alpha_o) dt \quad (16)$$

$$F_{Ti} = k_{p2}(r_i - r_o) + k_{d2} \frac{d}{dt}(r_i - r_o) + k_{i2} \int (r_i - r_o) dt \quad (17)$$

where $r_i = \sqrt{x_i^2 + y_i^2}$; $\alpha_i = \arctan(y_i/x_i)$; $r_o = \sqrt{x_o^2 + y_o^2}$; $\alpha_o = \arctan(y_o/x_o)$

The motion of robot in the vertical plane is controlled by the depth, pitch angle, and roll angle. The block

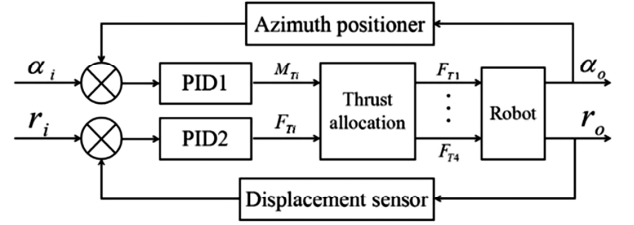


Figure 10. Block diagram of horizontal motion control.

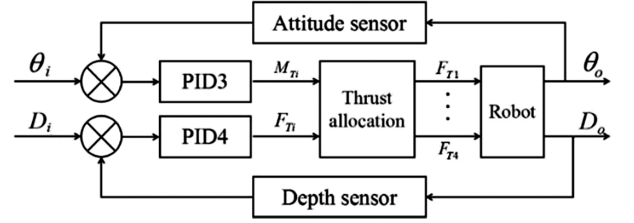


Figure 11. Block diagram of vertical motion control.

diagram of the algorithm is shown in Fig. 11. θ_i and θ_o are the input and output angle of robot, respectively. D_i and D_o are the displacement input and output of robot, respectively. The driving force and torque are given as follows:

$$M_{Ti} = k_{p1}(\theta_i - \theta_o) + k_{d1} \frac{d}{dt}(\theta_i - \theta_o) + k_{i1} \int (\theta_i - \theta_o) dt \quad (18)$$

$$F_{Ti} = k_{p2}(D_i - D_o) + k_{d2} \frac{d}{dt}(D_i - D_o) + k_{i2} \int (D_i - D_o) dt \quad (19)$$

5. Motion Stability Experiments on Land and Underwater

5.1 On-Land Gait Stability Experiments

We evaluated the motion of robot in terms of stability and velocity, and an NDI Polaris Vicra system was used

to evaluate the results, some of the control parameters were not varied during the co-simulations. The robot was programmed to move on a common mat floor; the experimental setup is shown in Fig. 12.

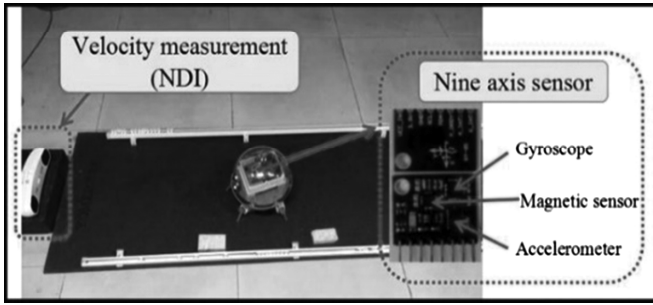


Figure 12. Experiments to evaluate the stability of the crawling gait.

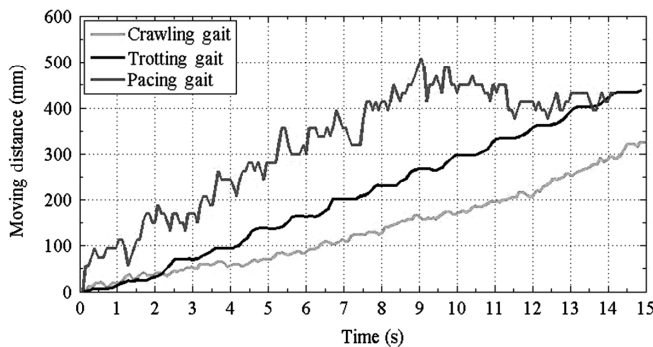


Figure 13. Displacement of the robot as it moves with different gaits.

The displacement of three on-land locomotion gaits of the PID-controlled robot are shown in Fig. 13. The velocity of the trotting gait increased quickly and became stable. The crawling gait was the slowest. The pacing gait was larger than the trotting gait due to the large yaw angle, the crawling gait was the most stable and the pacing gait was the least stable. Consequently, the crawling gait and trotting gait were selected as two common on-land movement gaits.

Figure 14 shows that the robot moved in a crawling gait, which is controlled using the PID method and the open-loop method. When the crawling gait was guided by the PID controller, it pitched and rolled in a stable manner, and the trajectory converged to the desired trajectory. The robot's walk was also less bumpy than when it was guided using the open-loop controller. When the PID-controlled robot moved with trotting gait, the pitch and roll angles were relatively small, and the yaw angle was large because the robot has only two legs in contact with the ground, as presented in Fig. 15, and the yaw angle gradually stabilized although there exist some deviations. The pacing gait is inherently unstable, and the yaw angle was slightly larger than it was with other gaits; but overall, the pacing motion was relatively stable.

These experimental results show that when these three on-land locomotion gaits are controlled using PID algorithm, the robot deviates far less from the desired trajectory, and its motion is smoother than when it is controlled by open-loop method. Overall, the motion on land meets our requirements. Consequently, PID controller is suitable for practical applications.

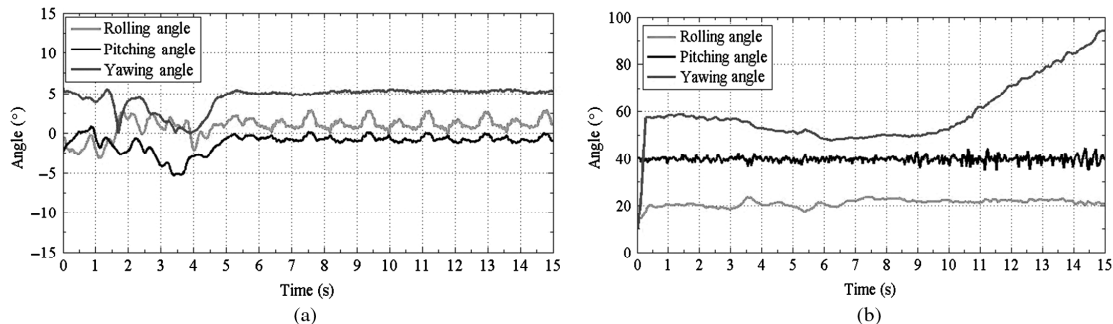


Figure 14. Amplitudes of the vibrations that occur when the robot moves with crawling gait.

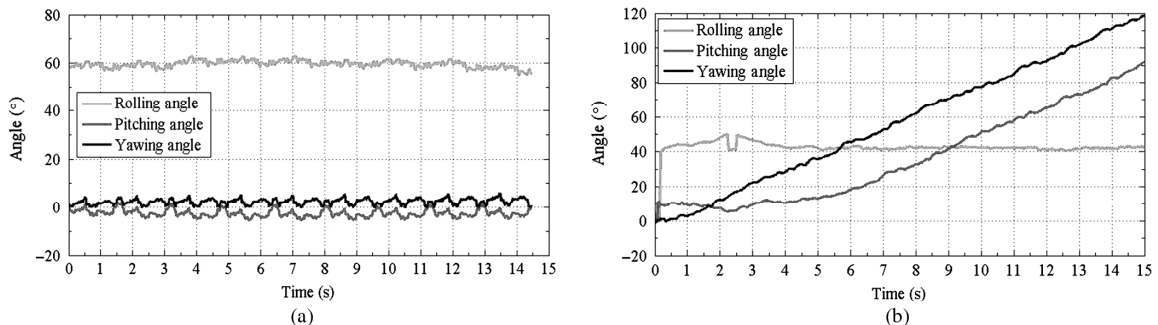


Figure 15. Attitude angle of the robot moves with trotting gait: (a) with PID control and (b) without PID control.

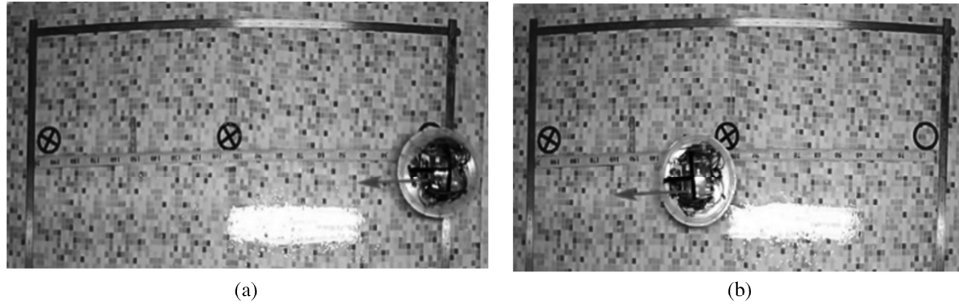


Figure 16. Underwater horizontal motion: (a) at 50 s and (b) at 3 s.

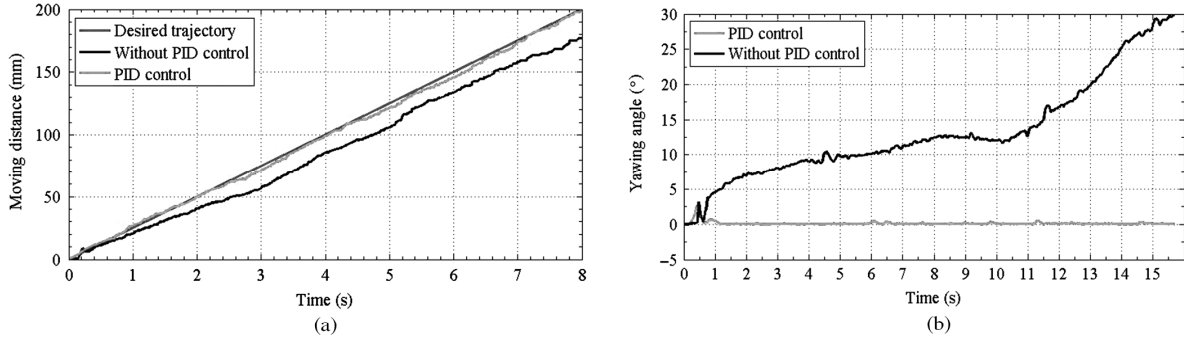


Figure 17. Trajectory comparison of the robot: (a) trajectory and (b) yawing angle.

5.2 Underwater Motion Stability Experiments

We evaluated the underwater performance of robot with both PID control and open-loop control experimentally. Each experiment was repeated 10 times. Control signals directed the robot move forward for 200 mm. The distance and angle were measured by using a ruler and an IMU sensor, respectively [24]. Figure 16 shows a video sequence of the horizontal motion; the red arrow indicates the moving direction.

The resulting trajectories and angles are shown in Fig. 17. As shown in Fig. 17(a), when the robot was guided by PID controller, the horizontal motion proceeds along the desired trajectory, although there were some deviations. However, when the robot was guided by open-loop controller, the errors were larger and the robot did not arrive at the target position. Fig. 17(b) shows the yaw angle of robot, the deviation at the start was large in both cases, and as the PID controller adjusts its control parameters, the deviation of the yaw angle gradually decreased and stabilized.

6. Conclusion

We aimed to improve the motion performance and stability of our amphibious spherical robot. We developed a PID closed-loop control method to guide the robot on land and underwater. To demonstrate the efficacy of the proposed method, we developed on-land and underwater co-simulations in an Adams and MATLAB/SIMULINK. Informed by the simulation results, we performed experiments on a common mat floor to evaluate the stability and velocity of three on-land gaits, and we also conducted horizontal underwater experiments to

evaluate our control method. Finally, we compared the performance of PID controller with the open-looped controller, and our proposed controller attained the best motion performance, with less deviation and vibration. In the future, we will improve on-land movement performance by developing new gaits and other adaptive control algorithm.

Appendix A Derivation of Robot Dynamic

According to Fig. 5, each leg consists of two links and two joints. Link 1 consists of L_1 and L_2 and can be rotated in the $X_bO_bY_b$ plane; Link 2 consists of L_3 and L_4 and can be rotated in the $Y_bO_bZ_b$ plane; $m_1, m_2, m_3,$ and m_4 are the corresponding qualities; l_i represents the length of the corresponding part; θ_1 and θ_2 represent generalized coordinates variables.

Kinetic energy and potential energy of Link 1 can be expressed as follows:

$$K_1 = \frac{1}{2} (m_1 + m_2) l_1^2 \dot{\theta}_1^2$$

$$P_1 = - (m_1 + m_2) g l_2$$

The centroid of Link 2 in Cartesian coordinate system can be expressed as follows:

$$\begin{cases} x_2 = (l_1 + l_3 \sin \theta_2 - l_4 \cos \theta_2) \cos \theta_1 \\ y_2 = (l_1 + l_3 \sin \theta_2 - l_4 \cos \theta_2) \sin \theta_1 \\ z_2 = -(l_2 + l_3 \cos \theta_2 + l_4 \sin \theta_2) \end{cases}$$

It can be obtained from the upper equation derivative:

$$\begin{cases} \dot{x}_2 = -\dot{\theta}_1 \sin \theta_1 (l_1 + l_3 \sin \theta_2 - l_4 \cos \theta_2) \\ \quad + \cos \theta_1 (l_3 \dot{\theta}_2 \cos \theta_2 + l_4 \dot{\theta}_2 \sin \theta_2) \\ \dot{y}_2 = \dot{\theta}_1 \cos \theta_1 (l_1 + l_3 \sin \theta_2 - l_4 \cos \theta_2) \\ \quad + \sin \theta_1 (l_3 \dot{\theta}_2 \cos \theta_2 + l_4 \dot{\theta}_2 \sin \theta_2) \\ \dot{z}_2 = l_3 \dot{\theta}_2 \sin \theta_2 - l_4 \dot{\theta}_2 \cos \theta_2 \end{cases}$$

$$\begin{aligned} \dot{v}_2 &= \dot{x}_2 + \dot{y}_2 + \dot{z}_2 = \dot{\theta}_1^2 l_1^2 + \dot{\theta}_1^2 l_3^2 \sin^2 \theta_2 + \dot{\theta}_1^2 l_4^2 \cos^2 \theta_2 \\ &+ 2l_1 l_3 \dot{\theta}_1^2 \sin \theta_2 - 2l_3 l_4 \dot{\theta}_1^2 \sin \theta_2 \cos \theta_2 \\ &- 2l_1 l_4 \dot{\theta}_1^2 \cos \theta_2 + l_3^2 \dot{\theta}_2^2 \sin^2 \theta_2 \\ &+ l_4^2 \dot{\theta}_2^2 \cos^2 \theta_2 (l_3 \dot{\theta}_2 \cos \theta_2 + l_4 \dot{\theta}_2 \sin \theta_2) \end{aligned}$$

So, the kinetic energy and potential energy of Link 2 can be expressed as follows:

$$\begin{aligned} K_2 &= \frac{1}{2} m v^2 = \frac{1}{2} (m_3 + m_4) v^2 \\ P_2 &= - (m_3 + m_4) g (l_2 + l_3 \cos \theta_2 + l_4 \sin \theta_2) \end{aligned}$$

The dynamic Lagrange equation of robot is given below:

$$\begin{aligned} L &= E_k - E_p = (K_1 + K_2) - (P_1 + P_2) \\ &= \left[\frac{1}{2} (m_1 + m_2) v_1^2 + \frac{1}{2} (m_3 + m_4) v_2^2 \right] + (m_1 + m_2) g l_2 \\ &\quad + (m_3 + m_4) g (l_2 + l_3 \cos \theta_2 + l_4 \sin \theta_2) \\ &= \frac{1}{2} (m_1 + m_2) l_1^2 \dot{\theta}_1^2 + \frac{1}{2} (m_3 + m_4) [\dot{\theta}_1^2 l_1^2 + \dot{\theta}_1^2 l_3^2 \sin^2 \theta_2 \\ &\quad + \dot{\theta}_1^2 l_4^2 \cos^2 \theta_2 + 2l_1 l_3 \dot{\theta}_1^2 \sin \theta_2 \\ &\quad - 2l_3 l_4 \dot{\theta}_1^2 \sin \theta_2 \cos \theta_2 - 2l_1 l_4 \dot{\theta}_1^2 \cos \theta_2 + l_3^2 \dot{\theta}_2^2 \sin^2 \theta_2 \\ &\quad + l_4^2 \dot{\theta}_2^2 \cos^2 \theta_2 - 2l_3 l_4 \dot{\theta}_2^2 \sin \theta_2 \cos \theta_2] \\ &\quad + (m_1 + m_2) g l_2 + (m_3 + m_4) g (l_2 + l_3 \cos \theta_2 + l_4 \sin \theta_2) \end{aligned}$$

Acknowledgement

This work was supported by National Natural Science Foundation of China (61503028 and 61773064). This research project was also partly supported by National Natural Science Foundation of China (61375094) and National High Tech. Research and Development Program of China (no. 2015AA043202).

References

- [1] S. Zhang, X. Liang, L. Xu, and M. Xu. Initial development of a novel amphibious robot with transformable fin-leg composite propulsion mechanisms, *Journal of Bionic Engineering*, 10(4), 2013, 434–445.
- [2] A.S. Boxerbaum, P. Werk, R.D. Quinn, and R. Vaidyanathan, Design of an autonomous amphibious robot for surf zone operation: Part I-Mechanical design for multi-mode mobility, *Proc. IEEE Conf. on Advanced Intelligent Mechatronics*, Monterey, CA, 2005, 459–1464.
- [3] Y. He, L. Shi, S. Guo, S. Pan, and Z. Wang, Preliminary mechanical analysis of an improved amphibious spherical father robot, *Microsystem Technologies*, 22(8), 2015, 1–16.

- [4] S. Pan, S. Guo, L. Shi, Y. He, Z. Wang, and Q. Huang, A spherical robot based on all programmable SoC and 3-D printing, *Proc. 2014 IEEE Conf. on Mechatronics and Automation*, Tianjin, 2014, 150–155.
- [5] S. Guo, Y. He, L. Shi, S. Pan, *et al.*, Modeling and experimental evaluation of an improved amphibious robot with compact structure, *Robotics and Computer Integrated Manufacturing*, 51, 2018, 37–52.
- [6] M. Li, S. Guo, H. Hirata, and H. Ishihara, Design and performance evaluation of an amphibious spherical robot, *Robotics and Autonomous Systems*, 64, 2015, 21–34.
- [7] L. Shi, S. Guo, S. Mao, C. Yue, M. Li, and K. Asaka, Development of an amphibious turtle-inspired spherical mother robot, *Journal of Bionic Engineering*, 10(4), 2013, 446–455.
- [8] S. Guo, L. Shi, S. Mao, and M. Li, Design and kinematic analysis of an amphibious spherical robot, *Proc. 2012 IEEE Conf. on Mechatronics and Automation*, Tianjin, Chengdu, 2012, 2214–2219.
- [9] S. Guo, J. Du, X. Ye, R. Yan, and H. Gao, The computational design of a water jet propulsion spherical underwater vehicle, *Proc. 2011 IEEE Conf. on Mechatronics and Automation*, Tianjin, 2014; Beijing, 2011, 2375–2379.
- [10] Z.G. Zhang, T. Masuda, H. Kimura, and K. Takase, Towards realization of adaptive running of a quadruped robot using delayed feedback control, *Proc. 2013 IEEE Conf. on Robotics and Automation*, Roma, 2007, 4325–4330.
- [11] C. Yue, S. Guo, L. Shi, and J. Du, Characteristics evaluation of the vertical motion of a spherical underwater robot, *Proc. 2014 IEEE Conf. on Robotics and Biomimetics*, Guangzhou, 2012, 759–764.
- [12] Y. Li, S. Guo, and C. Yue, Preliminary concept and kinematics simulation of a novel spherical underwater robot, *Proc. 2014 IEEE Conf. on Mechatronics and Automation*, Tianjin, 2014, 1907–1912.
- [13] X. Lin and S. Guo, Development of a spherical underwater robot equipped with multiple vectored water-jet-based thrusters, *Journal of Intelligent and Robotic Systems*, 67(3–4), 2012, 307–321.
- [14] S. Pan, L. Shi, S. Guo, P. Guo, Y. He, and R. Xiao, A low-power SoC-based moving target detection system for amphibious spherical robots, *Proc. 2015 IEEE Conf. on Mechatronics and Automation*, Beijing, 2015, 1116–1121.
- [15] Y. He, S. Guo, L. Shi, S. Pan, and P. Guo, Dynamic gait analysis of a multi-functional robot with bionic springy legs, *Proceedings of 2016 IEEE International Conference on Mechatronics and Automation*, Harbin, 2016, 689–694.
- [16] L. Bi, J. Guo, and S. Guo, Virtual prototyping technology-based dynamics analysis for an amphibious spherical robot, *Proc. 2015 IEEE Conf. on Information and Automation*, Lijiang, 2015, 2563–2568.
- [17] A. Delibasi, E. Zergeroglu, I.B. Küçükdemiral, and G. Cansever, Adaptive self-tuning control of robot manipulators with periodic disturbance estimation, *International Journal of Robotics and Automation*, 25(1), 2010, 48–56.
- [18] Z. Lu, Z. Ge, and W. Ding, Co-simulating quadruped weed-robot using ADAMS and MATLAB, *Mechanical Science and Technology for Aerospace Engineering*, 35(3), 2016, 375–380.
- [19] J. Wang, Y. Zhao, Y. Zhu, and Z. Ma, Coordinated simulation of trot gait for quadruped robot based on ADAMS and MATLAB, *Machine Tool & Hydraulics*, 43(3), 2015, 57–59.
- [20] D. Pan, F. Gao, Y. Miao, and R. Cao, Co-simulation research of a novel exoskeleton-human robot system on humanoid gaits with fuzzy-PID/PID algorithms, *Advances in Engineering Software*, 79, 2015, 36–46.
- [21] Y. Zhu and B. Jin, Compliance control of a legged robot based on improved adaptive control: Method and experiments, *International Journal of Robotics and Automation*, 31(5), 2016, 366–373.
- [22] S. Subramanian, T. George, and A. Thondiyath, Real-time obstacle avoidance for an underactuated flat-fish type autonomous underwater vehicle in 3D space space[J], *2012 Conf. on Instituto Argentino de Normalización y Certificación*, doi.10.2316/Journal.206.2014.4.206-4054, 2012, 1–16.
- [23] C. Yue, S. Guo, and M. Li, ANSYS FLUENT-based modeling and fluid dynamic analysis for a spherical underwater robot,

- [24] C.J. Lin, A GPU-based evolution algorithm for motion planning of a redundant robot, *International Journal of Robotics and Automation*, 2(2), 2017, 00015.

Biographies



Yanlin He received the B.S. degree in communication engineering from Lanzhou Jiaotong University, China, in 2011. Currently, she is a Ph.D. candidate in biomedical engineering at Beijing Institute of Technology, China. Her current research interests include amphibious spherical robot and multi-robot system. She has published about 25 refereed journal and conference papers in the

recent years.



Shuxiang Guo (IEEE SM'03) received the Ph.D. degree in mechatronics and systems from Nagoya University, Nagoya, Japan, in 1995. He is the chair professor in Key Laboratory of Convergence Medical Engineering System and Healthcare Technology, Ministry of Industry and Information Technology, Beijing Institute of Technology, China. He had been a full professor at the

Department of Intelligent Mechanical System Engineering, Kagawa University, Japan, since 2005. He has published about 500 refereed journal and conference papers. His current research interests include biomimetic underwater robots and medical robot systems for minimal invasive surgery, micro catheter system, *etc.*



Liwei Shi received the B.S. degree in mechanical engineering from Harbin Engineering University, China, in 2006, the M.S. and the Ph.D. degrees in intelligent machine system from Kagawa University, Japan, in 2009 and in 2012, respectively. He was a post-doctoral researcher in Kagawa University, Japan. Currently, he is an associate professor at the Beijing Institute of Technology,

he researches on underwater micro-robot utilizing artificial muscles, such as legged bio-inspired micro-robots, and spherical underwater robots, *etc.* He has published about 55 refereed journal and conference papers in the recent years.



Huiming Xing received the B.S. degree in automation from Qilu University of Technology, China, in 2013, and the M.S. degree in automation from Harbin Engineering University, China, in 2016, respectively. Currently, he is a Ph.D. candidate in automation at Beijing Institute of Technology, China. His current research interests include the navigation and control of amphibious spherical robot and multi-robot cooperation. He has published about 10 refereed journal conference papers in the recent years.



Zhan Chen received the B.S. degree in automation engineering from Beijing Information Science and Technology University, China, in 2016. Currently, he is an M.S. candidate in biomedical engineering at Beijing Institute of Technology, China. He researches on amphibious multi-robot formation control and communication.



Shuxiang Su received the B.S. degree in automation from the North China University of Technology, China, in 2016. Currently, he is a master from Beijing Institute of Technology, China. He researches on amphibious spherical robot and autonomous motion control of amphibious spherical robot. He has published about nine refereed journal and conference papers in the recent years.